Tuneable magnetic patterning of paramagnetic $Fe_{60}Al_{40}$ (at. %) by consecutive ion irradiation through pre-lithographed shadow masks

A. Varea,[1] E. Menéndez,[2] J. Montserrat,[3] E. Lora-Tamayo,[3] A. Weber,[4] L. J. Heyderman,[4] S. C. Deevi,[5] K. V. Rao,[6] S. Suriñach,[1] M. D. Baró,[1] K. S. Buchanan,[7] J. Nogués[8] and J. Sort[9,a)]

[1]*Departament de Física, Universitat Autònoma de Barcelona, 08193 Bellaterra, Spain*
[2]*Instituut voor Kern- en Stralingsfysica and INPAC, Katholieke Universiteit Leuven, Celestijnenlaan 200 D, BE-3001 Leuven, Belgium*
[3]*Institut de Microelectrònica de Barcelona (IMB-CNM), CSIC, Campus Universitat Autònoma Barcelona, E-08193, Bellaterra, Spain*
[4]*Laboratory for Micro- and Nanotechnology, Paul Scherrer Institut, 5232 Villigen PSI, Switzerland*
[5]*Research Center, Philip Morris USA, Inc., 4201 Commerce Road, Richmond, Virginia 23234, USA*
[6]*Department of Materials Science and Engineering, Royal Institute of Technology, S-10044, Stockholm, Sweden*
[7]*Department of Physics, Colorado State University, Fort Collins, Colorado 80523*
[8]*Institució Catalana de Recerca i Estudis Avançats (ICREA) and CIN2 (ICN-CSIC) and Universitat Autònoma de Barcelona, Catalan Institute of Nanotechnology, Campus de la UAB, E-08193 Bellaterra, Spain*
[9]*Institució Catalana de Recerca i Estudis Avançats (ICREA) and Departament de Física, Universitat Autònoma de Barcelona, E-08193 Bellaterra, Spain*

(Received 18 January 2011; accepted 9 April 2011; published online 13 May 2011)

Arrays of ferromagnetic circular dots (with diameters ranging from 225 to 420 nm) have been prepared at the surface of atomically ordered paramagnetic $Fe_{60}Al_{40}$ (at. %) sheets by means of ion irradiation through prelithographed poly(methyl methacrylate) (PMMA) masks. The cumulative effects of consecutive ion irradiation (using Ar^+ ions at 1.2×10^{14} ions/cm^2 with 10, 13, 16, 19 and 22 keV incident energies) on the properties of the patterned dots have been investigated. A progressive increase in the overall magneto-optical Kerr signal is observed for increasingly larger irradiation energies, an effect which is ascribed to accumulation of atomic disorder. Conversely, the coercivity, H_C, shows a maximum after irradiating at 16–19 keV and it decreases for larger irradiation energies. Such a decrease in H_C is ascribed to the formation of vortex states during magnetization reversal, in agreement with results obtained from micromagnetic simulations. At the same time, the PMMA layer, with an initial thickness of 90 nm, becomes progressively thinned during the successive irradiation processes. After irradiation at 22 keV, the remaining PMMA layer is too thin to stop the incoming ions and, consequently, ferromagnetism starts to be generated underneath the nominally masked areas. These experimental results are in agreement with calculations using the Monte-Carlo simulation *Stopping Range of Ions in Matter* software, which show that for exceedingly thin PMMA layers Ar^+ ions can reach the $Fe_{60}Al_{40}$ layer despite the presence of the mask. © *2011 American Institute of Physics*. [doi:10.1063/1.3590158]

I. INTRODUCTION

During the last decades, increasing demands from the fields of recording media and magnetic sensors have prompted the development of novel lithography methods to fabricate arrays of ferromagnetic (FM) dots with progressively smaller lateral dimensions.[1–5] Among the various procedures to prepare arrays of nanostructures are physical deposition of FM materials through prelithographed polymeric masks, chemical growth of FM phases inside nanoporous templates or selective etching of continuous FM films. To match specific technological demands, the properties of patterned magnetic materials often need to be precisely controlled. Typically, such control is accomplished either by varying the exact alloy composition or by modifying the shape and size of the lithographed structures.[1,6,7]

Alternatively, ion irradiation has been shown to be also an effective procedure to induce magnetic modifications in previously grown FM materials.[8] Indeed, ion irradiation has been employed to increase/reduce the value of saturation magnetization,[9] to induce soft magnetic behavior in otherwise hard magnetic materials (and viceversa),[10–12] to induce reorientation of the magnetic easy axis (from in-plane toward perpendicular-to-plane anisotropy direction)[13,14] or to vary the strength of interfacial coupling between FM and antiferromagnetic materials (i.e., to locally tune exchange bias properties).[15] Furthermore, ion irradiation can be used not only to tailor the magnetic properties of FM materials but also to induce ferromagnetism in certain paramagnetic materials. This occurs in some intermetallic alloys and austenitic stainless steels, which undergo structural transformations (from nonmagnetic to FM phases) when they become structurally disordered.[16–27] Disorder-induced magnetism has been actually reported in a number of transition-metal (TM)

a)Electronic mail: jordi.sort@uab.es.

intermetallics, such as FeAl,[16,17,19] $FePt_3$,[18] Ni_3Sn_2,[20] Fe_2AlMn,[21] CoAl,[22] or CoGa.[23] In these systems, the magnetism can be understood in terms of the local environment model, where the magnetic moment of a given TM atom depends on the number of nearest neighbor TM atoms.[24] Hence, the magnetic properties of these alloys (saturation magnetization, coercivity, etc.) depend on the amount of structural disorder. In turn, paramagnetic austenitic stainless steel transforms to FM martensite or FM expanded austenite under the action of mechanical stress[25] or N ion irradiation,[26,27] respectively.

It has been recently shown that focused ion beam (FIB) and ion irradiation through prelithographed poly(methyl methacrylate) (PMMA) masks can cause the necessary atomic disorder to induce ferromagnetism in the $Fe_{60}Al_{40}$ alloy.[16] However, while FIB is a rather slow patterning technique (i.e., the dots are written one by one, following an in-series approach), irradiation through PMMA masks also suffers from several drawbacks: the prepatterned PMMA resist layer needs to be thick enough to fully stop the incoming ions but if thickness is too large shadowing effects inside the patterned holes hinder the incoming ions from reaching the surface of $Fe_{60}Al_{40}$ alloy.

In this work, successive ion irradiation processes, using a constant ion fluence of 1.2×10^{14} ions/cm^2 and variable ion energies, from 10 to 22 keV, are performed at the surface of a $Fe_{60}Al_{40}$ sheet through arrays of holes (sub-500 nm in diameter) previously patterned on a PMMA layer by means of electron beam lithography. The aim of the work is twofold: (1) to investigate the evolution of the magnetic properties of the FM dots during the cumulative irradiation process and (2) to study how the PMMA mask withstands the various irradiation steps and establish the threshold energy beyond which PMMA becomes useless. Our results show that ferromagnetism in $Fe_{60}Al_{40}$ starts to be generated for incident ion energies of 13 keV. The Kerr signal progressively increases with the increase of ion energy as a consequence of the enhanced atomic disorder. However, for ion energies larger than 19 keV, the thickness of the PMMA layer is reduced by more than 60% and, consequently, the mask is no longer able to stop the incoming ions and ferromagnetism is then detected throughout the surface of the $Fe_{60}Al_{40}$ sheet.

II. EXPERIMENTAL

A fully dense 200 μm-thick Fe–40%Al-0.05%Zr-0.2%B (at. %) sheet, hereafter referred to as $Fe_{60}Al_{40}$, was prepared by cold rolling of prealloyed powders with the proper nominal composition. Prior to any irradiation process, mechanical polishing of the sheet was performed in order to eliminate surface oxides and to obtain mirrorlike appearance. The ferromagnetic behavior stemming from the atomic disorder induced during cold rolling and polishing was eliminated by annealing the sheet at 923 K for 30 min. This thermal treatment is sufficient to convert the disordered A2 phase into the atomically ordered B2 structure.[28] A 90 nm-thick poly(methyl methacrylate) (PMMA) resist layer was then spin coated onto the $Fe_{60}Al_{40}$ sheet surface and subsequently patterned using electron beam lithography to obtain arrays of circular dots, with diameters ranging from 225 to 420 nm. Consecutive ion irradiation through the PMMA shadow masks was carried out using Ar^+ ions with a fluence of 1.2×10^{14} ions/cm^2 and progressively larger energies (10, 13, 16, 19, and 22 keV), as illustrated in Fig. 1.

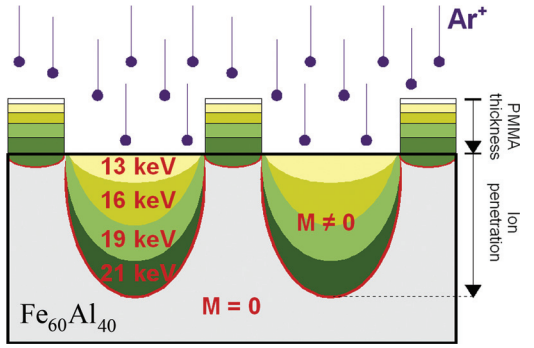

FIG. 1. (Color online) Schematic diagram showing a consecutive ion irradiation process, through a prelithographed PMMA mask deposited onto a $Fe_{60}Al_{40}$ sheet, using Ar^+ ions with progressively larger ion energies. Note that the extent of the generated ferromagnetic regions is proportional to the energy of the incident ions. The picture also illustrates that the thickness of the PMMA mask progressively decreases during the successive irradiation steps.

The ion damage caused during the cumulative irradiation process was modeled using MonteCarlo simulations by means of the Transport of Ions in Matter (TRIM) program included in the Stopping Range of Ions in Matter (SRIM) package.[29] The TRIM simulations compute the overall damage cascade caused by the recoiling atoms until their energy drops below the lowest displacement energy of any target atom. Essentially, TRIM allows obtaining the total number of target displacements (Fe plus Al displacements in $Fe_{60}Al_{40}$ and H plus C plus O displacements in PMMA) produced by one incident ion along its track. Note that a constant density of 1.2 g/cm^3 was assumed for PMMA and possible changes in density occurring during ion irradiation were not taken into account. Owing to the stochastic nature of ion-solid interactions, the total number of target displacement exhibits a distribution in depth. As shown in Fig. 2, for the range of energies used, the consecutive irradiation processes cause collisional damage down to around 30 nm in $Fe_{60}Al_{40}$ and 90 nm in PMMA.

The topography of the patterned dots was examined by scanning electron microscopy (SEM) and atomic force microscopy (AFM). Magnetic domain imaging was performed by magnetic force microscopy (MFM) using high sensitivity hard magnetic tips. Hysteresis loops were recorded at room temperature using longitudinal magneto-optic Kerr effect (MOKE), with a maximum applied magnetic field of 600 Oe and laser spot focused down to 3 μm.

Finally, micromagnetic simulations[30] were performed to determine the expected remanent states for the magnetic structures produced by the ion irradiation process. Three dimensional magnetic structures with an oblate spheroidal hemisphere shape with 350 nm in diameter were represented using $2.5 \times 2.5 \times 2.5$ nm^3 cells. Values for the saturation magnetization M_s were chosen based on previous work on ball milled $Fe_{60}Al_{40}$, i.e., 275 emu/cm^3 and 55 emu/cm^3 for

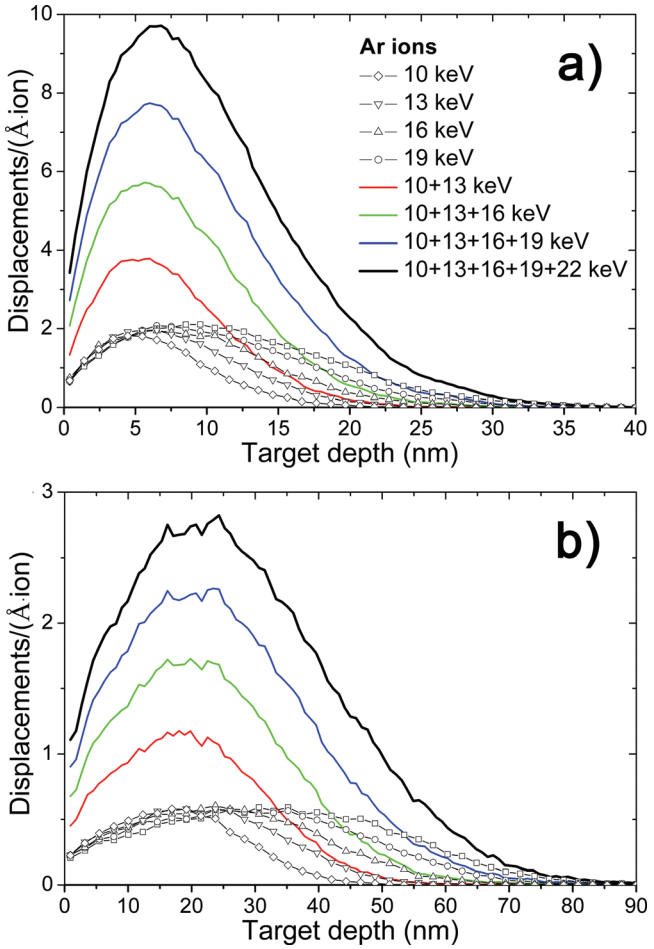

FIG. 2. (Color online) TRIM simulations of the target depth dependence of collision events (described by the number of target displacements per ion and traversed distance –given in Å–) in (a) the $Fe_{60}Al_{40}$ alloy and (b) the PMMA mask, after being irradiated using Ar^+ ions accelerated at 10, 13, 16, 19, and 22 keV. The effects of each irradiation step (with a single energy) and cumulative irradiations (with more than one energy) on the collisional damage are represented.

the most and less irradiated samples, respectively.[31] For the exchange parameter A a value of 1 μerg/cm^3 was used. The simulations were carried out using two different values for the anisotropy, 10^3 and $\sim 10^5$ erg/cm^3. The remanent states were calculated starting from initial states of (a) a vortex and (b) a uniform magnetization configuration with all spins oriented along the x-axis, also the easy axis, using a large damping coefficient ($\alpha = 1$).

III. RESULTS AND DISCUSSION

The MOKE measurements corresponding to the arrays of dots irradiated using 10 keV did not show any evidence of FM behavior, probably because in spite of the indicated surface ion damage at this energy (Fig. 2), the amount of structural disorder (and magnetism) in $Fe_{60}Al_{40}$ is exceedingly small to be detected by MOKE. Conversely, a small Kerr signal is observed after the arrays of dots have been further irradiated using Ar^+ ions with incident energy of 13 keV, i.e., after the cumulative effects of irradiating at 10 and 13 keV, (see MOKE loops for different dot sizes in Fig. 3). Interestingly, the amplitude of the Kerr signal progressively increases during the cumulative irradiation [Figs. 3(c) and 3(d)]. It is noteworthy that, for a given ion energy, the Kerr signal is larger for larger dot diameters. This trend is also observed if the laser spot is defocused, i.e., when increasing the amount of measured dots. Actually, normalization of the overall Kerr signal for the total area of measured dots does not cause an appreciable modification in the % Kerr signal. The origin of the dependence of the Kerr signal on the dot size is probably two-fold. On one hand, shadowing effects inside the PMMA lithographed holes are likely to occur during ion irradiation, particularly in the arrays of smaller dots, thus impeding a fraction of the incoming ions to reach the surface of the $Fe_{60}Al_{40}$ sheet and causing less induced ferromagnetism. On the other hand, one cannot rule out a shadowing effect during the MOKE measurements due to the 45° incidence of the polarized light. Namely, given the thickness of the PMMA mask, it is possible that not all the incoming light reaches the $Fe_{60}Al_{40}$ layer, particularly for the smallest dots.

The overall dependence of the Kerr signal on the energy of the incoming ions is shown in Fig. 4(a). The increase in Kerr signal is in agreement with the increase in the number of atomic displacements (i.e., ion damage) created in $Fe_{60}Al_{40}$ during ion irradiation [Fig. 2(a)]. Similar correlations between induced ferromagnetism and structural disorder were reported in $Fe_{60}Al_{40}$ subject to mechanical deformation experiments. Namely, an increase of the saturation magnetization was observed in $Fe_{60}Al_{40}$ powders during ball milling[31] and in bulk $Fe_{60}Al_{40}$ alloy under application of macroscopic compressive stress.[32,33]

Contrary to the saturation magnetization, the coercivity, H_C, does not depend in a simple and monotonic manner on the amount of structural disorder. In fact, although in nanostructured $Fe_{60}Al_{40}$ the uniaxial magnetic anisotropy has been shown to increase with the amount of atomic disorder,[34] H_C depends on the interplay between several factors (anisotropy, grain size, exchange interactions, etc.) which make its analysis more complex. In our case, H_C is found to show a maximum after successive irradiation using intermediate ion energies (16–19 keV), but it decreases for larger ion energies [see Fig. 4(b)]. The initial raise in H_C can be probably ascribed to the disorder-induced anisotropy increase. However, a constriction in the central part of the hysteresis loops also tends to appear during the cumulative ion irradiation process [Fig. 3(a) and 3(b)]. This constriction becomes more pronounced when larger ion energies are employed (i.e., when cumulative damage effects are increased). These peculiar loop shapes resemble those of magnetization reversal via vortex state formation. In such states, magnetization curling occurs for sufficiently low values of applied magnetic fields, resulting in a drop of the net magnetization. Magnetic curling is thus likely to be the reason for the observed decrease in coercivity, and it also causes a decrease in the remanent-to-saturation magnetization ratio (Fig. 3). It is noteworthy that magnetic vortex states are often encountered in disk-shaped FM dots composed of relatively soft magnetic materials and are particularly favored when the thickness of the FM material is sufficiently large.[35,36] Micromagnetic simulations were performed to shed light on the origin of the constricted shape of the hysteresis loops measured in the samples subjected to

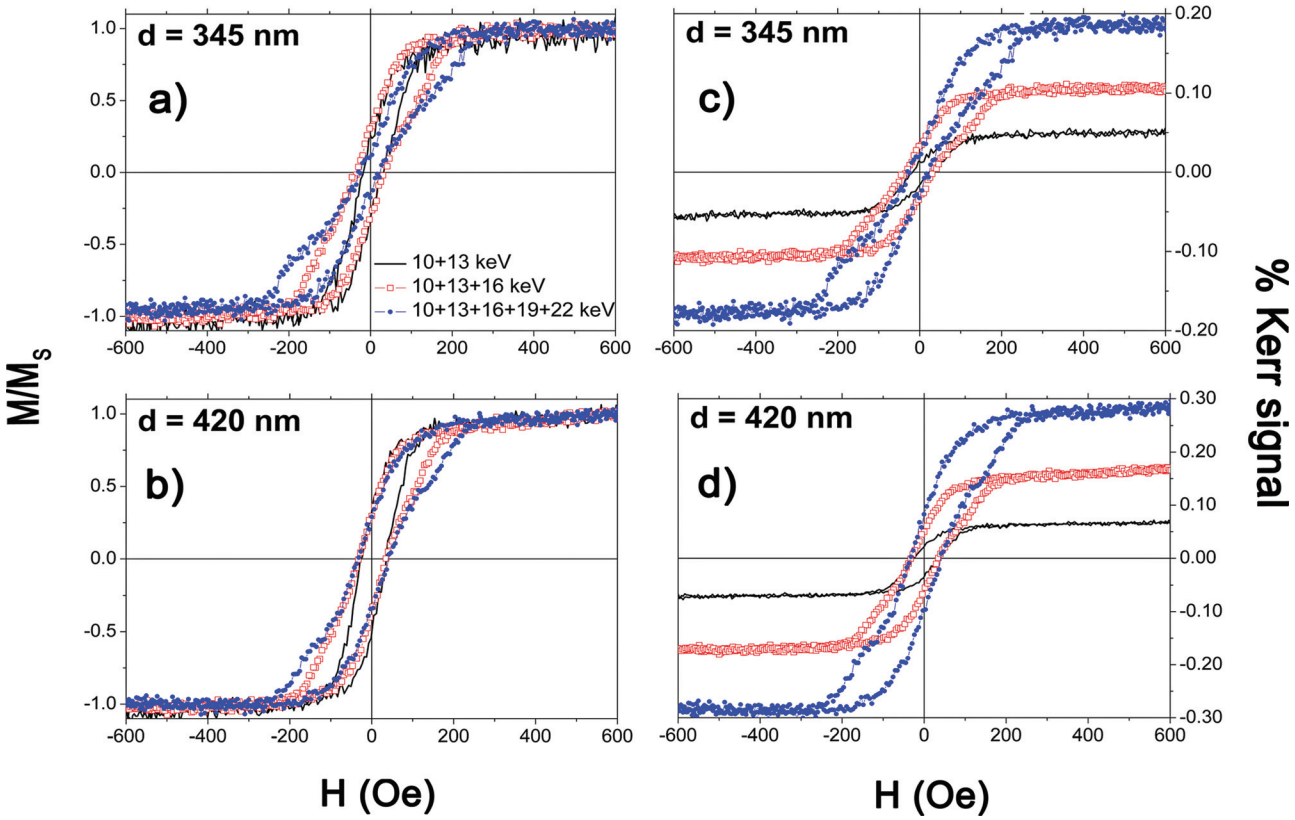

FIG. 3. (Color online) Normalized hysteresis loops, measured in longitudinal configuration by magneto-optic Kerr effect, corresponding to the arrays of magnetic dots with lateral size of (a) 345 nm and (b) 420 nm, obtained by successive ion irradiation processes. (c and d) The same hysteresis loops without being normalized.

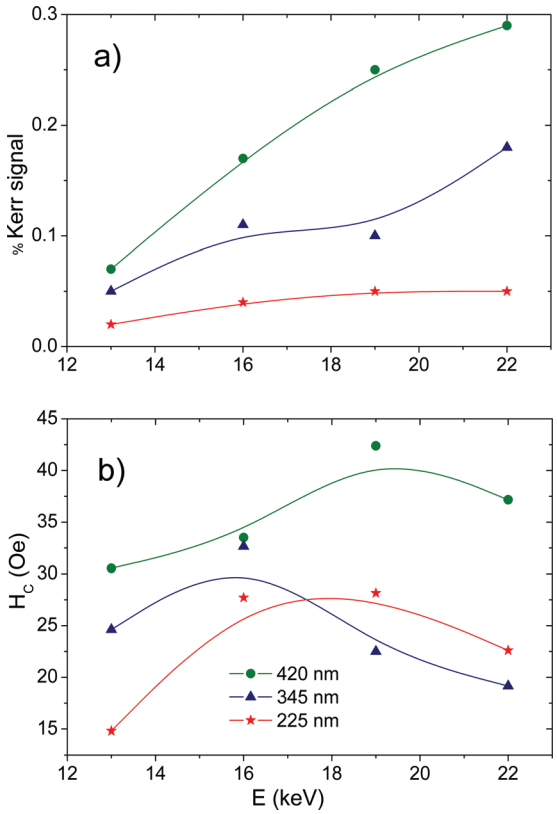

FIG. 4. (Color online) Variation of (a) the overall Kerr signal (which is proportional to the saturation magnetization) and (b) the coercivity, H_C, for each dot array, as a function of the incident ion energy during cumulative irradiation processes using incoming ions with 13, 16, 19, and 22 keV.

higher irradiation energies. Oblate spheroidal hemisphere shapes (350 nm in diameter) were used as simulation masks. Based on the SRIM calculations, the thicknesses of the oblate hemispheres were 30 nm and 15 nm for the most and least irradiated samples, respectively (see Fig. 2). Initially, the simulations were carried out using values of saturation magnetization $M_S = 275$ emu/cm^3 and anisotropy constant $K = 0.8 \times 10^7$ erg/cm^3 for the more irradiated sample and 55 emu/cm^3 and 0.02×10^7 erg/cm^3 for the low-energy irradiation condition. The spin configurations at the remanent state were first calculated starting from a uniform magnetization state along x (i.e., saturated state) and second starting from a vortex state. The results indicate that with these high magnetic anisotropies both structures settled into a single domain remanent state, independent of the initial spin configuration. When using weaker anisotropies, ($K = 1000$ erg/cm^3, which is of the same order of magnitude as for Permalloy), the less irradiated sample still settled into a single domain state [see Figs. 5(a) and 5(b)]. The energies associated with the vortex state were considerably higher and the single domain state was the clear ground state of this structure. Conversely, the spin configuration of the more irradiated sample, simulated using $K = 1000$ erg/cm^3, converged to a relaxed version of its initial state in each case and showed comparable energies for the single domain and vortex states (6.40×10^{-11} and 6.95×10^{-11} erg, respectively). Subsequently, we tested the effects of varying the M_s or the A values, increasing the former by 10% and decreasing the latter to 0.6 μerg/cm^3. In both cases the single domain state was found to be the ground state

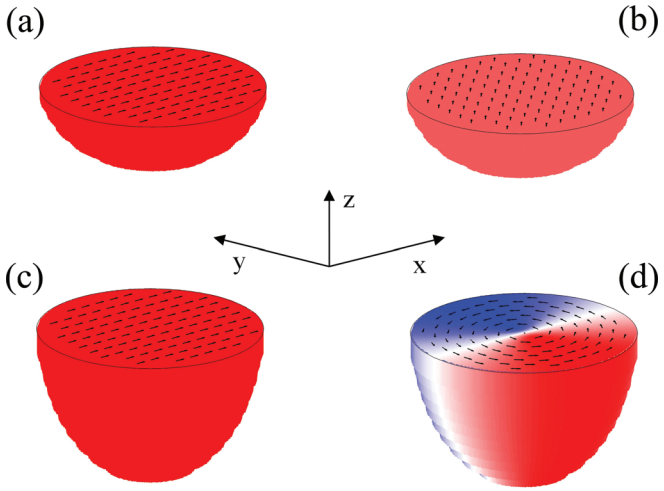

FIG. 5. (Color online) Spin configurations at remanence obtained using micromagnetic simulations for an oblate spheroidal hemisphere object, 350 nm in diameter, with low anisotropy. The arrows show the direction of the magnetic moment at the top surface and the colors correspond to the x-component of the magnetization where red (blue) indicates that the spins are aligned along the +x (−x) direction. (a and b) The relaxed magnetic states for 15-nm thick structures, corresponding to the sample irradiated at low energies. These spin configurations in Figs. 5(a) and 5(b) were relaxed from a uniform initial state along x and a vortex state, respectively. Both show calculated remanent states that are single domain. (c and d) The relaxed spin configurations of the spheroidal hemisphere object with thickness of 30 nm, i.e., corresponding to the most irradiated sample, where the calculations were started from a uniform (x) and a vortex configuration, respectively. In both cases the relaxed spin configurations reflect the initial conditions and have similar energies. These configurations are obtained using reasonable values of saturation magnetization, exchange parameter and anisotropy (see text for details).

for the less irradiated sample, whereas the vortex state was found to be the ground state for the more irradiated sample. In the latter, the energy became approximately 26% lower for the vortex as compared to the single domain when M_S was increased by 10%, and 42% lower when A was decreased to 0.6 μerg/cm^3. Thus, the simulations show that a vortex reversal process is likely for the most irradiated samples [see Fig. 5(c) and 5(d)], provided the net anisotropy is weak and assuming values for the saturation magnetization similar to those previously reported in the literature.[31] The less irradiated samples, however, are expected to maintain single domain configurations. The relatively low values of K are probably realistic since the random directions of the induced structural disorder will have the net effect of lowering the value of the effective magnetic anisotropy.

The local character of the ferromagnetism induced by ion irradiation was examined by MFM. Some MFM images

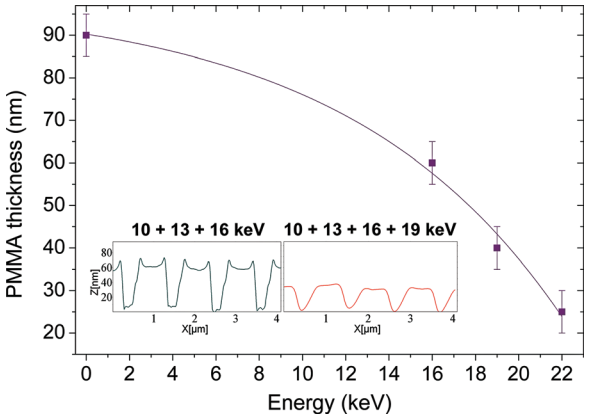

FIG. 7. (Color online) Dependence of the PMMA thickness during consecutive irradiation processes using ions with progressively larger energies. The insets show the topological profiles, obtained by atomic force microscopy (AFM), of the arrays of dots with initial diameter of 345 nm, after being irradiated using 16 keV and 19 keV.

of the $Fe_{60}Al_{40}$ sheets irradiated up to 16 keV, obtained at remanence after applying a magnetic field of 600 Oe, are shown in Fig. 6. Dark and bright areas are observed inside the irradiated circles, evidencing magnetic stray fields. No contrast is observed outside the dots, which indicates that the PMMA shadow mask is capable of blocking the incident ions during cumulative ion irradiation using energies of 10, 13, and 16 keV. Note that for this energy the PMMA thickness has been reduced from 90 nm to approximately 60 nm, as evaluated by atomic force microscopy (see Fig. 7). According to Fig. 2(b), ion damage in the PMMA after ion irradiation using $10+13+16$ keV is mainly concentrated within the upper 60 nm. Consequently, in spite of the PMMA thickness reduction not enough ions reach the $Fe_{60}Al_{40}$ sheet to induce magnetism. Hence, the lack of magnetic contrast between the patterned dots in $Fe_{60}Al_{40}$ is in agreement with the Monte-Carlo simulations results.

The thickness of the PMMA resist layer continues to decrease when further irradiation steps, using larger ion energies, are performed. Indeed, as shown in Fig. 7, the PMMA layer is only about 25 nm thick after ion irradiation at 22 keV. At the same time, the PMMA resist becomes progressively hardened and some cracks appear as a result of the cumulative irradiation process (see Fig. 8). This shrinkage and hardening of PMMA during ion irradiation is a well-known effect, and it is related to the outgassing and molecular ejection of H_2, CH_3, CH_4, H_2O, C_2H_2, and CO_2 species from the polymer, an effect which leads to an increase of carbon content in the residual material.[37,38] MOKE measurements of

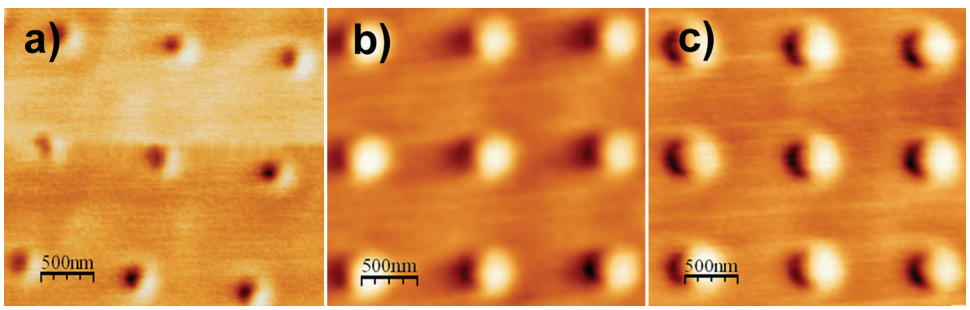

FIG. 6. (Color online) Magnetic force microscopy (MFM) images of arrays of circular dots, with diameters: (a) 225 nm, (b) 345 nm, and (c) 420 nm, obtained after three consecutive irradiation processes using Ar^+ ions with 10, 13, and 16 keV. Note that a magnetic field of 600 Oe was applied, prior to imaging, along the sheet plane direction.

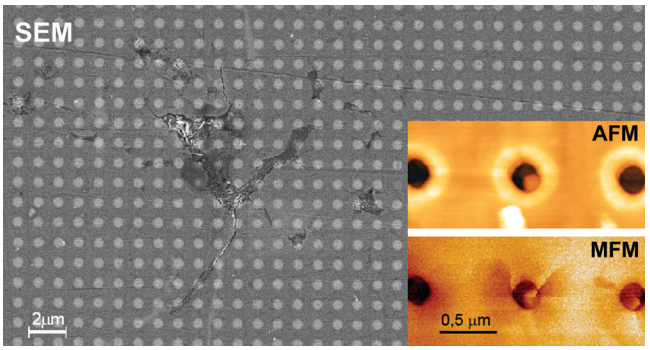

FIG. 8. (Color online) Scanning electron microscopy (SEM) image of the array of dots ($\Phi = 420$ nm) obtained after consecutive ion irradiation using 13 keV + 16 keV + 19 keV + 22 keV. The inset compares an atomic force microscopy, AFM, and the corresponding magnetic force microscopy, MFM, image of these dots, revealing that magnetic contrast is observed both inside and in-between the dots.

the sample irradiated up to 22 keV revealed ferromagnetic behavior not only in the arrays of dots, but also when focusing the laser spot outside of the lithographed arrays. Concomitantly, MFM measurements show the existence of domain walls surrounding the patterned dots (see inset in Fig. 8). This indicates that, for the ion fluence used in this work (1.2×10^{14} ions/cm^2) and the initial PMMA thickness of 90 nm, successive irradiations up to 19 keV Ar^+ ions is the maximum tolerable by the PMMA mask layer.

IV. CONCLUSIONS

In conclusion, consecutive ion irradiation processes through prelithographed PMMA masks, employing variable ion energies ranging between 10 and 22 keV, have been used to induce and subsequently tailor the ferromagnetic properties of sub-500 nm patterned magnetic circles. The obtained results show that, similar to varying the dot aspect ratio or material composition, cumulative ion irradiation is a suitable method to tailor the magnetic properties (saturation magnetization or coercivity) of small ferromagnetic objects. In particular, a transition from squarelike to vortexlike hysteresis loops is observed for ion energies beyond 16 keV, suggesting the occurrence of magnetic curling effects which result in a decrease in the coercivity and the remanent magnetization of the dots. In turn, an upper limit for the incoming ion energy is established. These results are of technological relevance for the implementation of lithography methods based on ion irradiation using polymer layers as masks. In particular, applications such as magnetic sensors, separators, recording media or magnetic logic circuits[39] could benefit from the use of this patterning approach.

ACKNOWLEDGMENTS

This work was partially financed by the MAT2007-61629 and MAT2010-20616-C02 research grants from the Spanish MICINN and the 2009-SGR-1292 project from the Generalitat de Catalunya. The authors acknowledge Dr. O. Liedke and Professor J. Fassbender for their fruitful discussions and comments. Part of the work was carried out using the capabilities of the ICTS/Clean Room of Micro and Nano-fabrication of the IMB-CNM (CSIC), under the auspices of the GICSERV-5 call (NGG-106 project) funded by the Spanish MICINN. E.M. thanks the Fund for Scientific Research–Flanders (FWO) for financial support. M.D.B. was partially supported by an ICREA ACADEMIA award. K.S.B. acknowledges support from Grant No. NSF DMR 0907706.

[1]J. I. Martín, J. Nogués, K. Liu, J. L. Vincent, and I. K. Schuller, J. Magn. Magn. Mater. **256**, 449 (2003).
[2]C. A. Ross, H. I. Smith, T. Savas, M. Schattenburg, M. Farhoud, M. Hwang, M. Walsh, M. C. Abraham, and R. J. Ram, J. Vac. Sci. Technol. B **17**, 3168 (1999).
[3]B. D. Terris, T. Thomson, J. Phys. D: Appl. Phys. **38**, R199 (2005).
[4]M. M. Aziz, D. M. Newman, A. Sidwell, M. L. Wears, and C. D. Wright, Nanotechnol. **21**, 505303 (2010).
[5]A. O. Adeyeye and N. Singh, J. Phys. D: Appl. Phys. **41**, 153001 (2008).
[6]S. Y. Chou, Proc. IEEE **85**, 652 (2007).
[7]R. Skomski, J. Phys.: Cond. Matter. **15**, R841 (2003).
[8]J. Fassbender and J. McCord, J. Magn. Magn. Mater. **320**, 579 (2008).
[9]J. Fassbender, J. von Borany, A. Mücklich, K. Potzger, W. Möller, J. McCord, L. Schultz, and R. Mattheis, Phys. Rev. B **73**, 184410 (2006).
[10]B. D. Terris, L. Folks, D. Weller, J. E. E. Baglin, A. J. Kellock, H. Rothuizen, and P. Vettiger, Appl. Phys. Lett. **75**, 403 (1999).
[11]T. Hasegawa, G. Q. Li, W. Pei, H. Saito, S. Ishio, K. Taguchi, K. Yamakawa, N. Honda, K. Ouchi, T. Aoyama, and I. Sato, J. Appl. Phys. **99**, 053505 (1999).
[12]J.-P. Adam, J.-P. Jamet, J. Ferré, A. Mougin, S. Rohart, R. Weil, E. Bourhis, and J. Gierak, Nanotechnol. **21**, 445302 (2010).
[13]C. Chappert, H. Bernas, J. Ferre, V. Kottler, J. P. Jamet, Y. Chen, E. Cambril, T. Devolder, F. Rousseaux, V. Mathet, and H. Launois, Science **280**, 1919 (1998).
[14]S. Konings, J. Miguel, J. Goedkoop, J. Camarero, and J. Vogel, J. Appl. Phys. **100**, 033904 (2006).
[15]A. Mougin, S. Poppe, J. Fassbender, B. Hillebrands, G. Faini, U. Ebels, M. Jung, D. Engel, A. Ehresmann, and H. Schmoranzer, J. Appl. Phys. **89**, 6606 (2001).
[16]E. Menéndez, M. O. Liedke, J. Fassbender, T. Gemming, A. Weber, L. J. Heyderman, K. V. Rao, S. C. Deevi, S. Suriñach, M. D. Baró, J. Sort, and J. Nogués, Small **5**, 229 (2009).
[17]J. Fassbender, M. O. Liedke, T. Strache, W. Möller, E. Menéndez, J. Sort, K. V. Rao, S. C. Deevi, and J. Nogués, Phys. Rev. B **77**, 174430 (2008).
[18]S. Maat, A. J. Kellock, D. Weller, J. E. E. Baglin, and E. E. Fullerton, J. Magn. Magn. Mater. **265**, 1 (2003).
[19]J. Sort, A. Concustell, E. Menéndez, S. Suriñach, K. V. Rao, S. C. Deevi, M. D. Baró, and J. Nogués, Adv. Mater. **18**, 1717 (2006).
[20]G. F. Zhou and H. Baker, Phys. Rev. B **49**, 12507 (1994).
[21]I. Baker, D. Wu, M. Wittmann, and P. R. Munroe, Mater. Charact. **52**, 209 (2004).
[22]L. M. Di, H. Bakker, and F. R. de Boer, Physica B **182**, 91 (1992).
[23]L. M. Di, H. Bakker, Y. Tamminga, and F. R. de Boer, Phys. Rev. B **44**, 2444 (1991).
[24]G. K. Wertheim, V. Jaccarino, J. H. Wernick, and D. N. E. Buchanan, Phys. Rev. Lett. **12**, 24 (1964).
[25]J. Sort, A. Concustell, E. Menéndez, S. Suriñach, M. D. Baró, J. Farran, and J. Nogués, Appl. Phys. Lett. **89**, 032509 (2006).
[26]E. Menéndez, J.-C. Stinville, C. Tromas, C. Templier, P. Villechaise, J.-P. Rivière, M. Drouet, A. Martinaviîcius, G. Abrasonis, J. Fassbender, M. D. Baró, J. Sort, and J. Nogués, Appl. Phys. Lett. **96**, 242509 (2010).
[27]G. Abrasonis, J. P. Rivière, C. Templier, A. Declémy, L. Pranevicius, and X. Milhet, J. Appl. Phys. **97**, 083531 (2005).
[28]A. Hernando, X. Amils, J. Nogués, S. Suriñach, M. D. Baró, and M. R. Ibarra, Phys. Rev. B **58**, 11864 (1998).
[29]J. F. Ziegler, J. P. Biersac, and U. Littmark, *The Stopping and Range of Ions in Solids* (Pergamon, New York, 1985).
[30]M. R. Scheinfein, M. R. LLG Micromagnetics Simulator, TM, available at http://llgmicro.home.mindspring.com/.
[31]X. Amils, J. Nogués, S. Suriñach, M. D. Baró, and J. S. Muñoz, IEEE Trans. Magn. **34**, 1129 (1998).
[32]D. Wu and I. Baker, Mater. Sci. Eng. A **329-331**, 334 (2002).
[33]E. Menéndez, J. Sort, M. O. Liedke, J. Fassbender, S. Suriñach, M. D. Baró, and J. Nogués, New J. Phys. **10**, 103030 (2008).

[34]X. Amils, J. Nogués, S. Suriñach, and M. D. Baró, J. Magn. Magn. Mater. **203**, 129 (1999).
[35]N. Dao, S. L. Whittenburg, and R. P. Cowburn, J. Appl. Phys. **90**, 5235 (2001).
[36]K. Y. Guslyenko, J. Nanosci. Nanotechnol. **8**, 2745 (2008).
[37]L. Torrisi, Rad. Eff. Def. Sol. **145**, 285 (1998).
[38]F. Schrempel, Y.-S. Kim, and W. Witthuhn, Appl. Surf. Sci. **189**, 102 (2002).
[39]J. O. Klein, E. Belhaire, C. Chappert, R. Cowburn, D. Read, and D. Petit, Int. J. Electron. **95**, 249 (2008).